Electronic Supplementary Information

Subtle Polymorphism of Zinc Imidazolate Frameworks: Temperature-Dependent Ground States in the Energy Landscape Revealed by Experiment and Theory

Christian A. Schröder,[a] *Igor A. Baburin,*[b] *Leo van Wüllen,*[c] *Michael Wiebcke,*[*,a] *and Stefano Leoni*[*,b]

[a] Institut für Anorganische Chemie, Leibniz Universität Hannover, Callinstrasse 9, 30167 Hannover, Germany

[b] Institut für Physikalische Chemie und Elektrochemie, Technische Universität Dresden, Mommsenstrasse 13, 01062 Dresden, Germany

[c] Institut für Physik, Universität Augsburg, Universitätsstrasse 1, 86159 Augsburg, Germany

Table of Contents

0. Computational Details

I. Structure optimization

I.1

The SIESTA program package[1a] was used to perform conjugate-gradient relaxations on [Zn(im)$_2$] structures (**coi** and **zni**). During relaxation both atomic coordinates and cell shape were allowed to change. The metric of the tetragonal crystal family was initially constrained to improve the convergence by controlling angle deviations from those required by crystal symmetry. The geometry was relaxed to residual forces smaller than 0.02 eV/Å with a stress tolerance less than 0.1 GPa. Calculations including only Γ-point of the Brillouin zone with an energy cutoff of 250 Ry ensured convergence of the electronic part for both structures. Subsequently, convergence of the total energy with respect to the number of *k*-points was carefully checked. The calculations were performed within the GGA approximation using Perdew-Burke-Ernzerhof (PBE) exchange-correlation functional.[2a] Norm-conserving Trouiller-Martins pseudopotentials[3] represented the core electrons. The polarized double-ζ (DZP) basis set was the same as that already applied in a previous paper on [Zn(im)$_2$] polymorphs.[4]

Framework topology	Energy / eV/[Zn(im)$_2$] **GGA-PBE, DZP**	Energy difference / eV/[Zn(im)$_2$]	Optimized cell vectors* **(GGA-PBE, DZP) /** Å	Relaxed Volume of a primitive cell / Å^3
coi	–3761.1552	0.0000	*a* = 22.1118; *c* = 13.1310	3210.0811
zni	–3761.0920	0.0632	*a* = 22.7645; *c* = 12.5822	3260.1893

*Experimental values: **coi** (*a*= 22.7482(3); *c* = 13.0168(3) Å at 298 K); **zni** (*a* = 23.5028(4); ***c*** = 12.4607(3) Å at 298 K)[5].

I.2

The Kohn-Sham equations (without spin polarization) were solved using the plane-wave pseudo-potential approach, as implemented in the PWscf/Quantum-ESPRESSO computer package[1b]. A non-local van der Waals correlation functional was used to account for dispersion interactions. The Vydrov and Van Voorhis functional[2b] in its revised form[2c] were used. The parametrization of ultrasoft pseudopotentials allowed us to limit the kinetic-energy cutoff for the plane-wave basis set to 60 Ry (Density cutoff: 400 Ry). The same parameter choice was made for the Im-Im dimer, see below. With respect to GGA, we noticed an elongation of the H-H non-bonded equilibrium distances and an overall slight increase of the volume by ~2.5 %.

Framework topology	Energy eV/[Zn(im)$_2$] **rVV10**	Energy difference eV/[Zn(im)$_2$]	Optimized cell vectors*/ Å	Relaxed Volume of a primitive cell / Å^3
coi	-6518.6523	0.0000	*a* = 22.2843; *c* =13.2453	3288.7590
zni	-6518.6360	0.0163	*a* = 23.1909; *c* = 12.5463	3373.8060

II. Molecular Dynamics (MD) Simulations

Variable cell shape isothermic (Nose), isobaric (Parrinello-Rahman) MD simulations were carried out with the SIESTA package.[1a] The equations of motion were integrated with a modified Verlet algorithm, with a self-consistent set of equations for the Nose and Parrinello-Rahman variables. The moments of inertia of Nose and Parrinello-Rahman variables were set to 150 Ry·fs^2.Four sets of MD runs were performed at T = 500, 600, 620 and 650 K. The zero-temperature, relaxed **coi** structure was used as an input configuration. The initial 1-1.5 ps where typically disregarded in the data analysis. GGA (PBE) functional[2a] was used to compute the forces on the atoms. The calculations were based on a 272 atoms primitive cell. The system was thermalised for 1 ps, followed by >10 ps integration time. Temperature fluctuations were within ±9%. The timestep was 1 fs. For computational efficiency single-ζ basis set was employed. At 620 K the averaged a and c parameters (with respect to the conventional body-centred I cell) were 20.84 and 13.48 Å, respectively. At 650 K their averaged values amount to 20.51 and 13.17 Å, respectively.

III. Comparison GGA-PBE vs. van der Waals (rVV10)

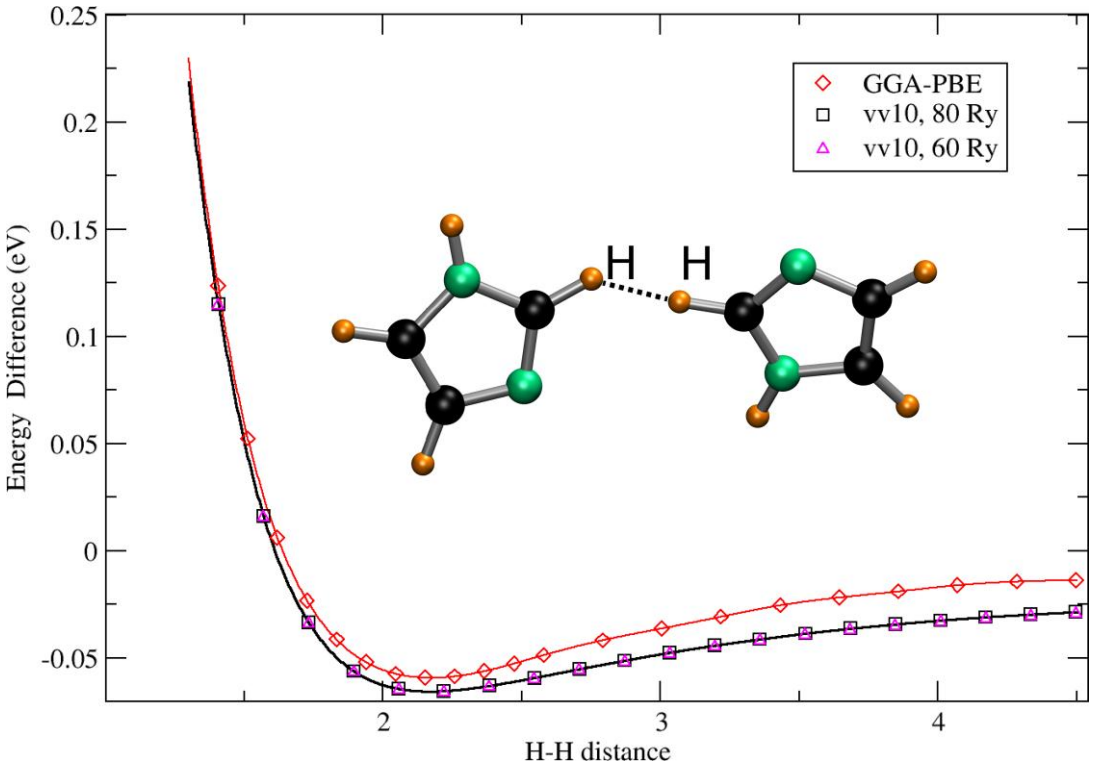

Fig. S1.a: Comparison of the binding energy for the Im-Im dimer along the H···H reaction coordinate. The GGA-PBE results (SIESTA) display a minimum at 2.17 Å and compare very well with the profile calculated based on the revised VV10 van der Waals functional (minimum at 2.20 Å), slight differences showing up in the "more dispersive" region.

IV. Molecular Dynamics Data Analysis - Descriptors

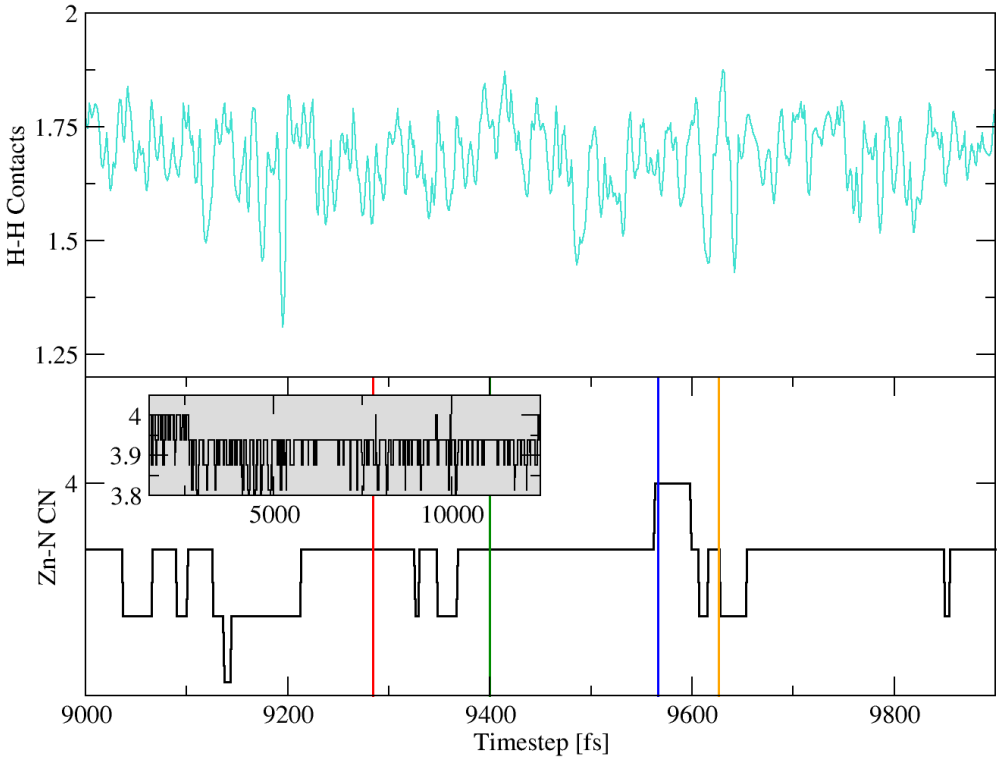

Fig. S1.b: Evolution of relevant quantities along the MD simulation run at 377 °C, characterized by a more frequent trigonal-bipyramidal Zn center formation, coupled with the shortening of the non-bonded H···H contacts. Lower Panel: evolution of the average Zn-N coordination number (CN) between 9.0 and 9.9 ps. At 9.6 the CN=4 corresponds to the simultaneous formation of a trigon and a trigonal-bipyramid, and represents a reactive event. Lower Panel, Inset: Evolution of the CN between 1.5 and 12.5 ps. A typical configuration displays one trigonal Zn per cell, which is shown by the CN staying at 3.9375 after 2.1 ps. This situation is accompanied by volume compression, influencing H...H contacts. Upper panel: Shortest H···H distances between 9.0 and 9.9 ps. Fluctuation of shortest distances correspond to reduced Zn-N CNs, which indicates a correlation in time. The response of the system to temperature is a lowering of the average H···H below 1.7 towards an activation of Zn-N bonds.

V. Molecular Dynamics Data Analysis – H···H Supramolecular Scaffolding and Zn Trigonal-Bipyramidal Center Formation

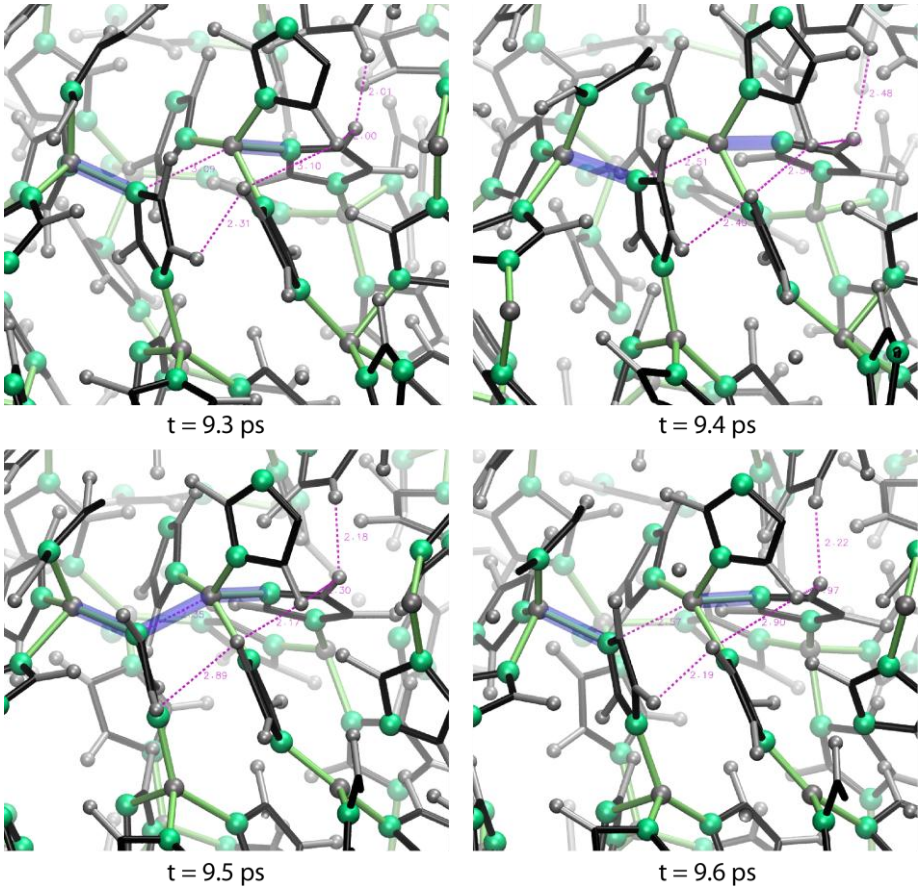

Fig. S1.c: Formation of Zn trigonal centers and fluctuations of H-H non-bonded distances. The correlation between changes in coordination spheres around Zn centers and H-H average distance shortenings, already pointed out in Fig S1.b, manifest itself in a cooperative mechanism, which involves the formation of a web of H-H contacts (purple dotted lines) at times of Zn-N bond elongations. This web is sensibly affected by volume contractions. Notice the 5-coordinated geometry at t= 9.5 ps. The 4 strokes in Fig. S1.b (red, green, blue and orange) refer to the configuration sequence shown here. The snapshots refer to the MD simulation run performed at 377°C.

VI. Molecular Dynamics Data Analysis – Thermal Contraction I

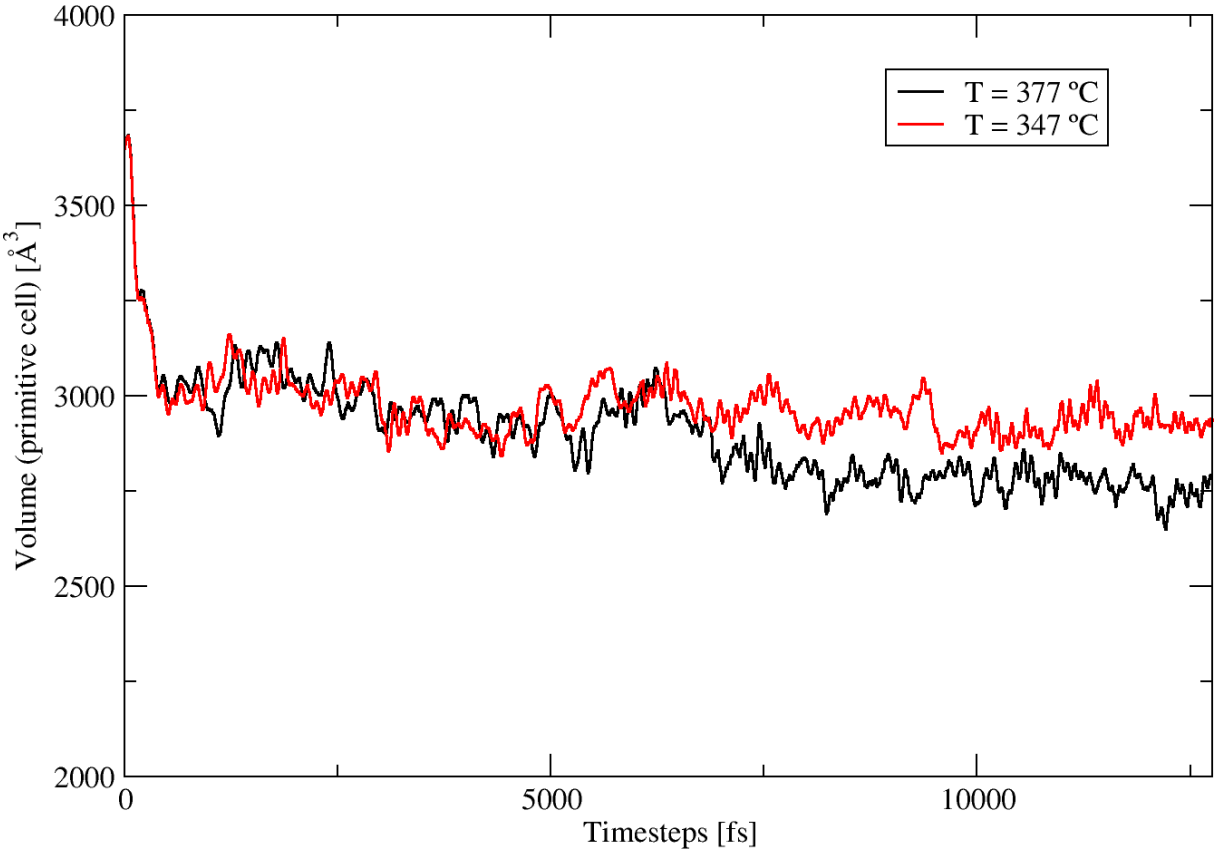

Fig. S1.d: Evolution of the volume for two MD runs at different temperatures (347°C and 377°C). The volume contracts in response to temperature: after 6500 fs the volume varies within a small window, at no point black and red curves overlap. The profiles refer to simulations performed in the primitive 272 atoms cell, as indicated above. The starting configuration was the zero-temperature, relaxed **coi** structure.

VI. Molecular Dynamics Data Analysis – Thermal Contraction II

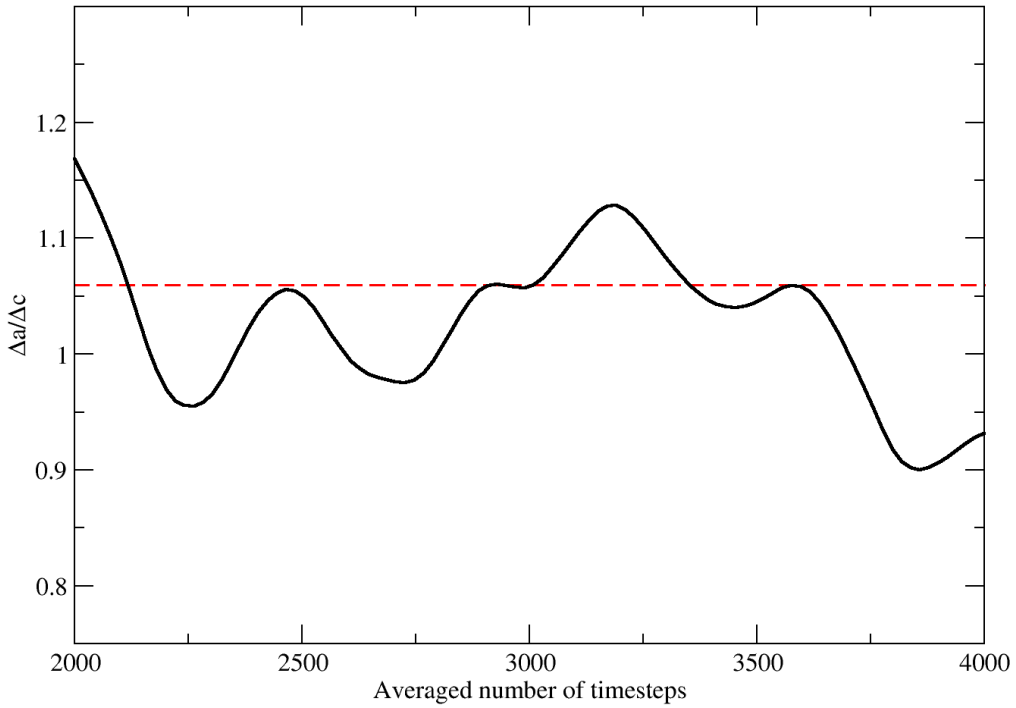

Fig. S1.e: Evolution of D=(Δa/Δc) as a function of the number of timesteps over which time-averaged quantities are calculated. The segment of the MD simulations runs considered corresponds to the final parts of the trajectory, where the variations of the structural parameters are small (Fig. S1.d, 8700-12700 fs). The broken line indicate the average value D=1.06.

Table S1.a:Averaged a, c cell parameters and the volume at T = 347 and 377 °C, respectively, and the resulting D ratios as a function of the number of timesteps considered (left column) for time-averaging.

	D=Δa/Δc	a_{347}Å	a_{377}Å	c_{347}Å	c_{377}Å	V_{347}Å^3	V_{377}Å^3
2000	1.17	20.87	20.49	13.49	13.17	2937.52	2763.86
2080	1.1	20.85	20.49	13.50	13.17	2935.12	2764.16
2500	1.05	20.83	20.49	13.50	13.18	2929.62	2767.47
3000	1.06	20.84	20.51	13.48	13.17	2926.27	2770.59
3500	1.04	20.84	20.52	13.47	13.17	2923.49	2772.29
4000	0.93	20.85	20.54	13.48	13.15	2929.91	2774.24

1. General Methods of Characterization

Differential scanning calorimetry (DSC) measurements were performed on a Perkin Elmer Pyris 1 DSC apparatus without using a purge gas. A ramp rate of 10 $K \cdot min^{-1}$ was applied. For calibration indium metal was used (T_m = 156.6 °C, ΔH_m = 28.45 $kJ \cdot mol^{-1}$). The dry powder was placed in an Aluminum pan sealed with a punctured cover.
Enthalpies were calculated using the Pyris DSC software for Windows, version 3.50.

High-resolution powder X-ray diffraction (XRD) patterns were recorded using a Stoe STADI-P transmission diffractometer using monochromatised $CuK_{\alpha 1}$ radiation (wavelength 1.54056 Å) and a linear position sensitive detector.

For the variable-temperature XRD studies the same instrument was equipped with a Stoe high-temperature oven. The dry powder was filled into a quartz glass capillary with an outer diameter of 0.5 mm which was left unsealed. XRD patterns were measured at constant temperatures in temperature intervals of 5 K in the 2θ range 10–25°. Measurement of each pattern took 150 min.
Each diffraction pattern was evaluated using the program TOPAS (Bruker AXS). Indexing and lattice constant determination was performed by full pattern profile decomposition applying the Le Bail method. Bragg reflections were fitted using a split Pearson VII function.

Thermogravimetric analysis (TGA) and differential thermal analysis (DTA) measurements were performed on a Netzsch Thermal Analyser STA 429 in flowing air with a ramp rate of 5 $K \cdot min^{-1}$. Samples were filled into corundum crucibles.

Solid State ^{13}C NMR spectra were recorded on a Bruker Avance III spectrometer operating at 7 T with a resonance frequency of 75.5 MHz. The ^{13}C CPMAS (cross polarization magic angle spinning) NMR experiment was performed at room temperature employing a spinning speed of 10 kHz, RF amplitudes of 50 kHz and TPPM decoupling. TMS was used as an external reference for the ^{13}C chemical shifts.

2. Synthesis of $[Zn(im)_2]$-coi

Commercially available chemicals were used without further purification: $Zn(OAc)_2 \cdot 2H_2O$ (Sigma-Aldrich, reagent grade), imidazole (Sigma-Aldrich, ≥ 99 %), pyridine (Sigma-Aldrich, ≥ 99 %), ethanol (Sigma-Aldrich, ≥ 98 %).

For the synthesis a procedure reported by Tian *et al.* was adopted:[6] Typically a solution containing 1.36 g (20.0 mmol) of imidazole in 30 mL (0.51 mol) of ethanol was poured into a solution containing 1.82 g (8.3 mmol) of $Zn(OAc)_2 \cdot 2H_2O$ in 30 mL (0.37 mol) of pyridine (total molar ratio: Zn : imidazole : pyridine : ethanol = 1 : 2.4 : 45 : 62). Upon mixing a bulky amorphous phase formed which dissolved within approximately2 h while the $[Zn(im)_2 \cdot 0.5py]$-**neb** phase precipitated (see section 5., synthesis of $[Zn(im)_2 \cdot 0.5py]$-**neb**). After stirring for 24 h at room temperature 4 mL of the mixture were placed in a sealed glass tube and treated solvothermally at 140 °C for 24 h using an oil bath. During this treatment the solution was vigorously stirred. The upper part of the tube was allowed to stand out of the oil bath creating reflux-like conditions. After the mixture was cooled to room temperature the white $[Zn(im)_2]$-**coi** powder was separated from the solution by filtration and washed with ethanol. Yield was 60 % with regard to Zn.

When the solvothermal treatment of such mixtures was carried out under static conditions, either in a circulating air oven or in an oil bath, only mixtures of **coi** and **zni** could be obtained.

3. Characterization of [Zn(im)$_2$]-coi

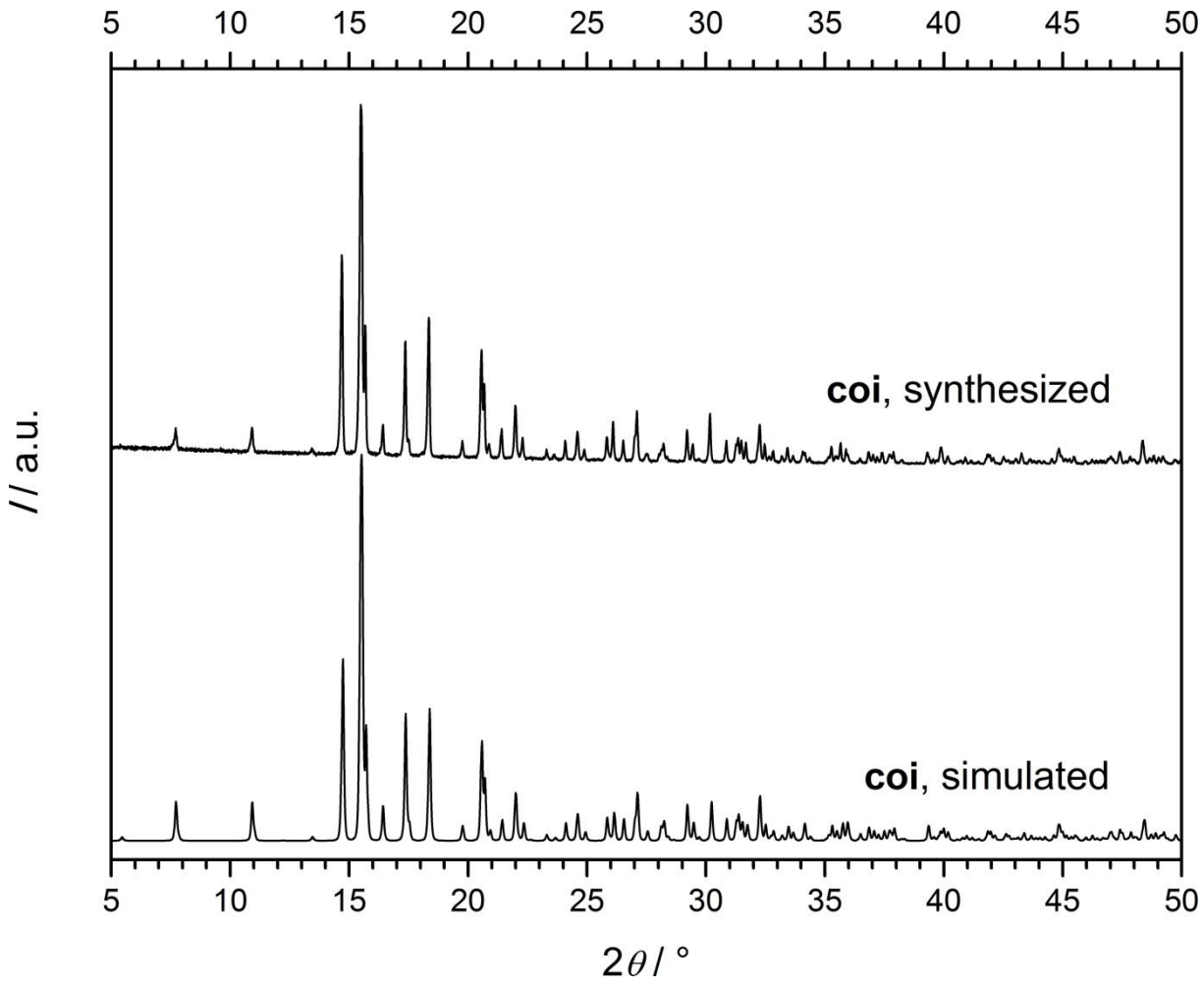

Fig. S2:XRD pattern of[Zn(im)$_2$]-**coi** recorded at room temperature. The material was obtained after solvothermal treatment under reflux-like conditions of a stirred [Zn(im)$_2$·0.5py]-**neb**-containing mixture (see section 2.). For comparison an XRD pattern simulated from structure data is also shown proving that pure-phase [Zn(im)$_2$]-**coi** was obtained.[6]

Without stirring the **neb** mixture during solvothermal treatment it was not possible to obtain a pure-phase as shown in the following figures.

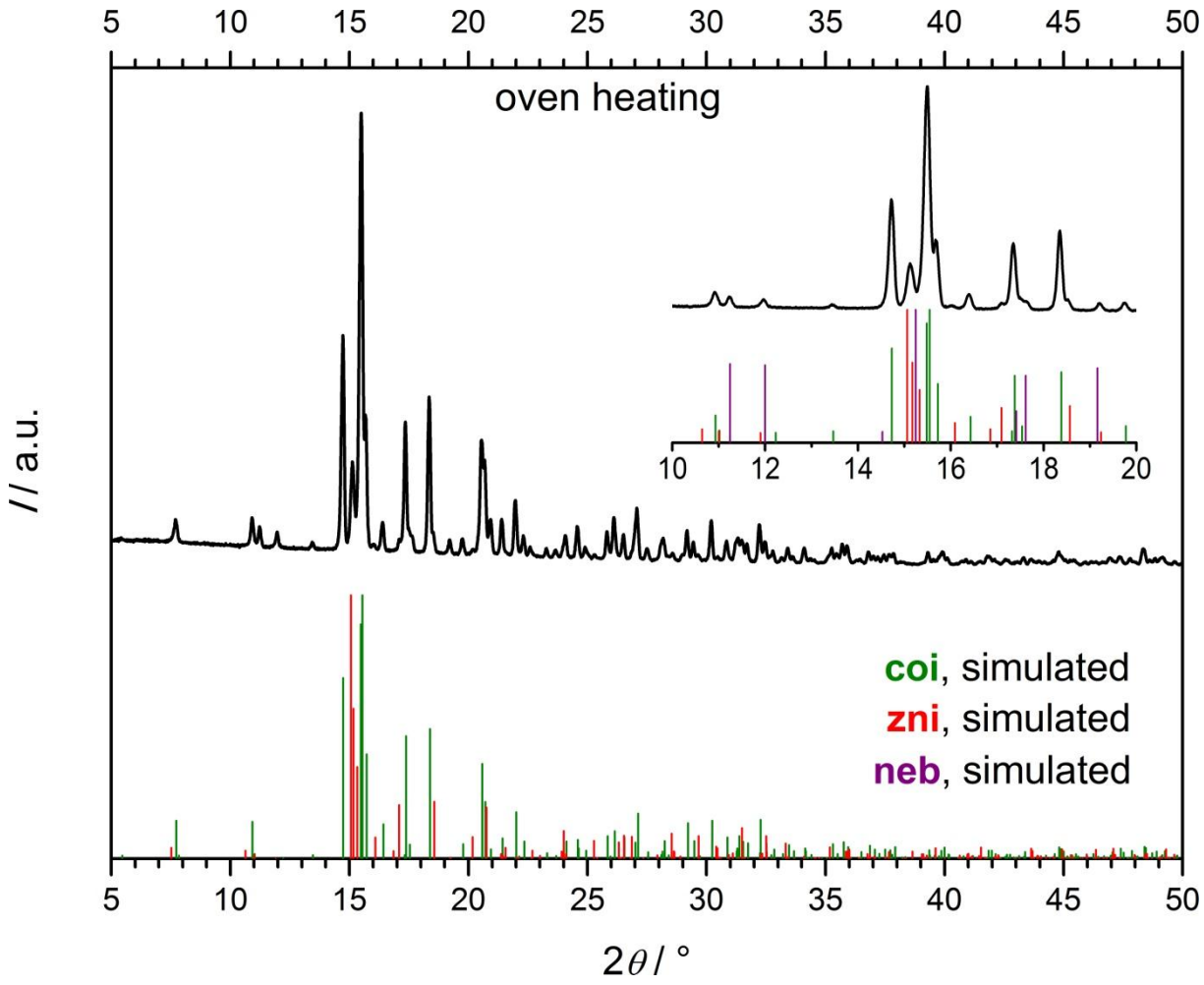

Fig. S3: XRD pattern (black curve) of a mixture of [Zn(im)$_2$]-**coi** and [Zn(im)$_2$]-**zni** obtained after solvothermal treatment under static conditions in a circulating air oven (140 °C, 24 h). For comparison simulated XRD patterns of **coi** and **zni**[5] are shown in the lower panel. Weak reflections at 11.2 ° and 12.0 ° 2θ can be assigned to residual amounts of [Zn(im)$_2$·0.5py]-**neb** (see inset).

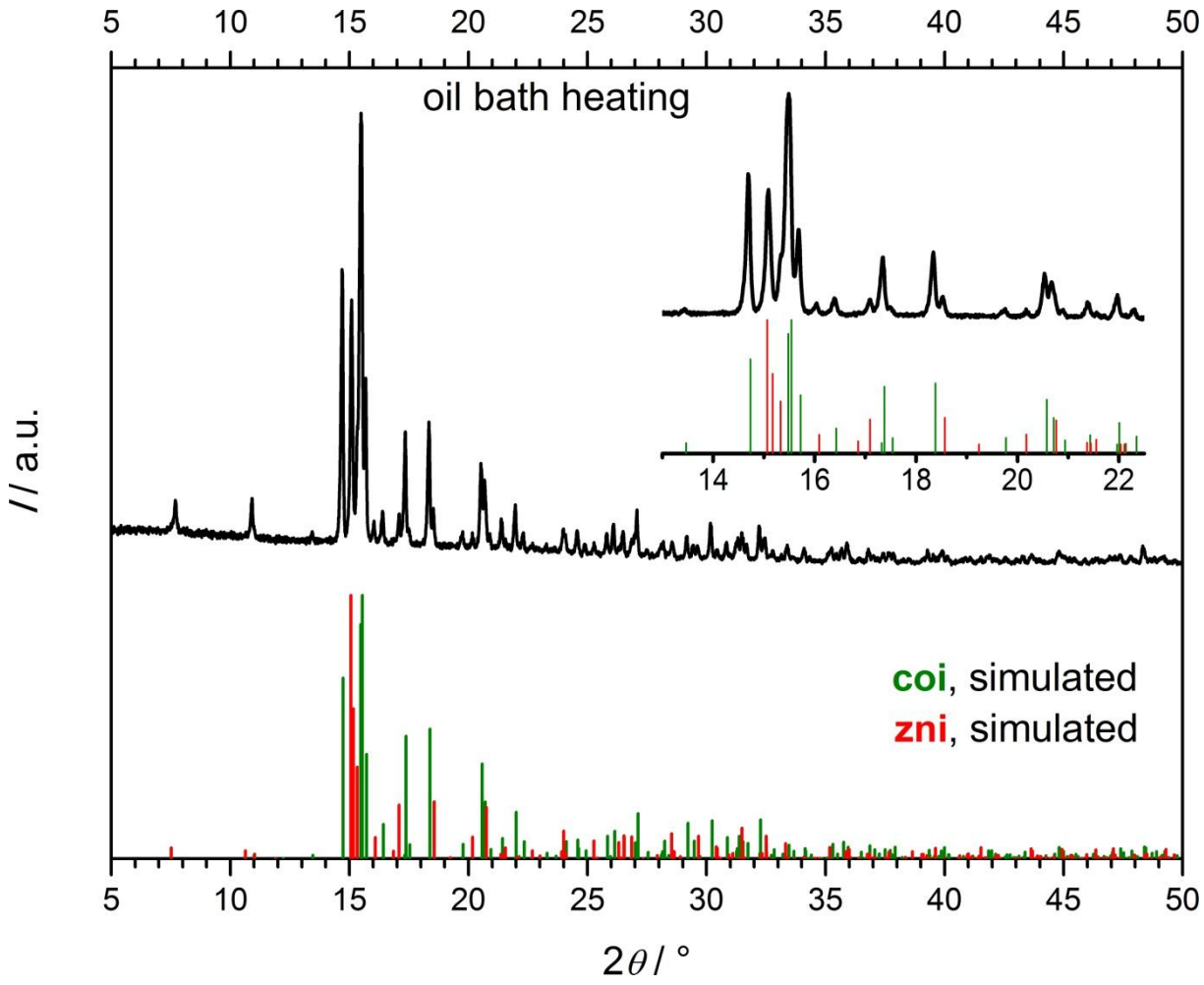

Fig. S4:XRD pattern (black curve) of a mixture of [Zn(im)$_2$]-**coi** and [Zn(im)$_2$]-**zni** obtained after solvothermal treatment under static conditions in an oil bath (140 °C, 24 h). For comparison simulated XRD patterns of **coi** as well as **zni**[5] are shown in the lower panel.
A detailed view for the region of the most intense reflections is provided by the inset.

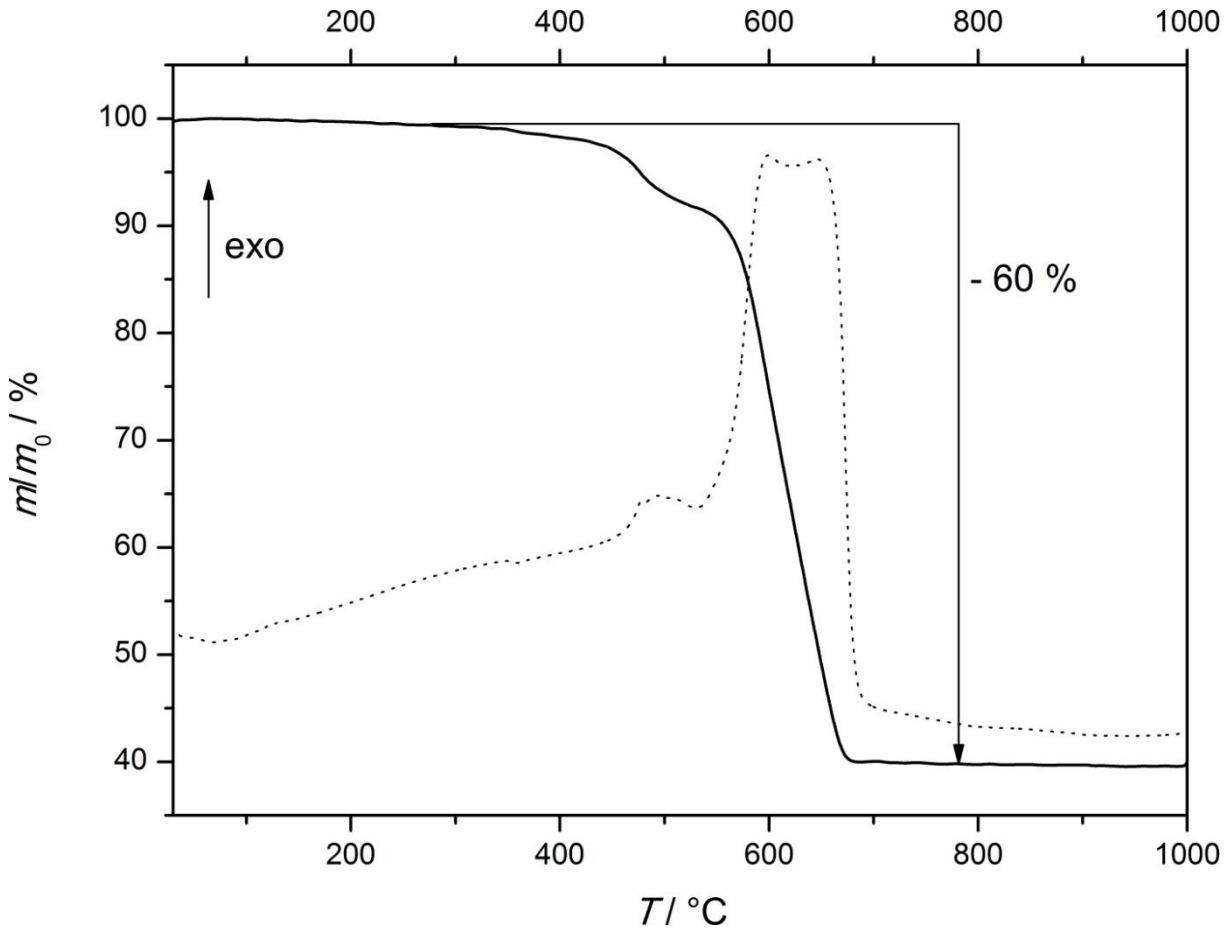

Fig. S5: TGA (solid line) and DTA (dotted line) curves measured from a $[Zn(im)_2]$-**coi** sample which was previously activated by thermal treatment at 250 °C for 2 h. The observed total mass loss (60 %) is in a good agreement with the calculated ones (60 %) assuming the decomposition of **coi** into solid hexagonal ZnO (as verified by XRD) and volatile components. As-synthesized (non-activated) **coi** powder usually contains a minor amount of solvent (ca. 1 %), TGA not shown.

4. *In situ* Energy Dispersive X-ray Diffraction (EDXRD)

To monitor the transition from [Zn(im)$_2$·0.5py]-**neb** to [Zn(im)$_2$]-**coi** under solvothermal conditions time-resolved *in situ* EDXRD experiments were performed at beamline F3 at light source DORIS III at DESY (Hamburg, Germany). This beamline receives white synchrotron radiation with an energy range of 8–56 keV and a maximum photon flux at approximately 16 keV. A fixed angle solid-state germanium detector was used to record the diffracted radiation. A detector angle of $\theta \approx 1.5°$ was chosen to place the most intense reflections of [Zn(im)$_2$·0.5py]-**neb** as well as the most intense reflections of **coi** close to maximum flux. Silver behenate powder was used to calibrate the detector angle.

To obtain good intensities statistics during the EDXRD experiments reaction mixtures with a composition of Zn : imidazole : pyridine : ethanol = 2 : 4.8 : 45 : 62 were used which is two times more concentrated with regard to the standard procedure described in section 2. Solvothermal reactions were carried out in sealed borosilicate glass tubes with a diameter of 9 mm and a volume of 7 mL. The tubes were filled with 4 mL of the **neb**-containing mixture and placed in an aluminium block which was kept at a temperature of 140 °C using a circulating oil heater. The solution was vigorously stirred during the experiment. The time between placing the tubes in the aluminium block and starting the measurement was approximately30 s. Recording time for each EDXRD spectrum was 120 s.

The intensity data were normalised to the baseline intensity. The profiles of the Bragg peaks were fitted with a pseudo Voigt function using the software TOPAS (Bruker AXS). The extent of reaction $\beta(t)$ was calculated as the ratio of the integrated intensity for a given time, t, to the maximum integrated intensity ,I_{max}. In case of the **neb** phase $\beta(t)$ was calculated from the sum of the integrated intensities of the 111 and 220 Bragg peaks ,I_{max} was calculated from the mean integrated intensity of the first five spectra. In case of the **coi** phase $\beta(t)$ was calculated from the sum of the integrated intensities of the 112, 400 and 231 Bragg peaks. To determine I_{max} the integrated intensities of the last five spectra were averaged.

5. Synthesis of [Zn(im)$_2$·0.5py]-neb

Commercially available chemicals were used without further purification: Zn(OAc)$_2$·2H$_2$O (Sigma-Aldrich, reagent grade), imidazole (Sigma-Aldrich, ≥ 99 %), pyridine (Sigma-Aldrich, ≥ 99 %), ethanol (Sigma-Aldrich, ≥ 98 %).
Typically a solution containing 1.36 g (20.0 mmol) of imidazole in 30 mL (0.51 mol) of ethanol was poured into a solution containing 1.82 g (8.3 mmol) of Zn(OAc)$_2$·2H$_2$O in 30 mL (0.37 mol) of pyridine (total molar ratio: Zn : imidazole : pyridine : ethanol = 1 : 2.4 : 45 : 62). Upon mixing, a bulky, amorphous phase was formed which dissolved within approximately2 h while the [Zn(im)$_2$·0.5py]**-neb** phase precipitated. After 24 h the white powder was separated from the mixture and washed with ethanol.

6. Characterization of [Zn(im)$_2$·0.5py]-neb

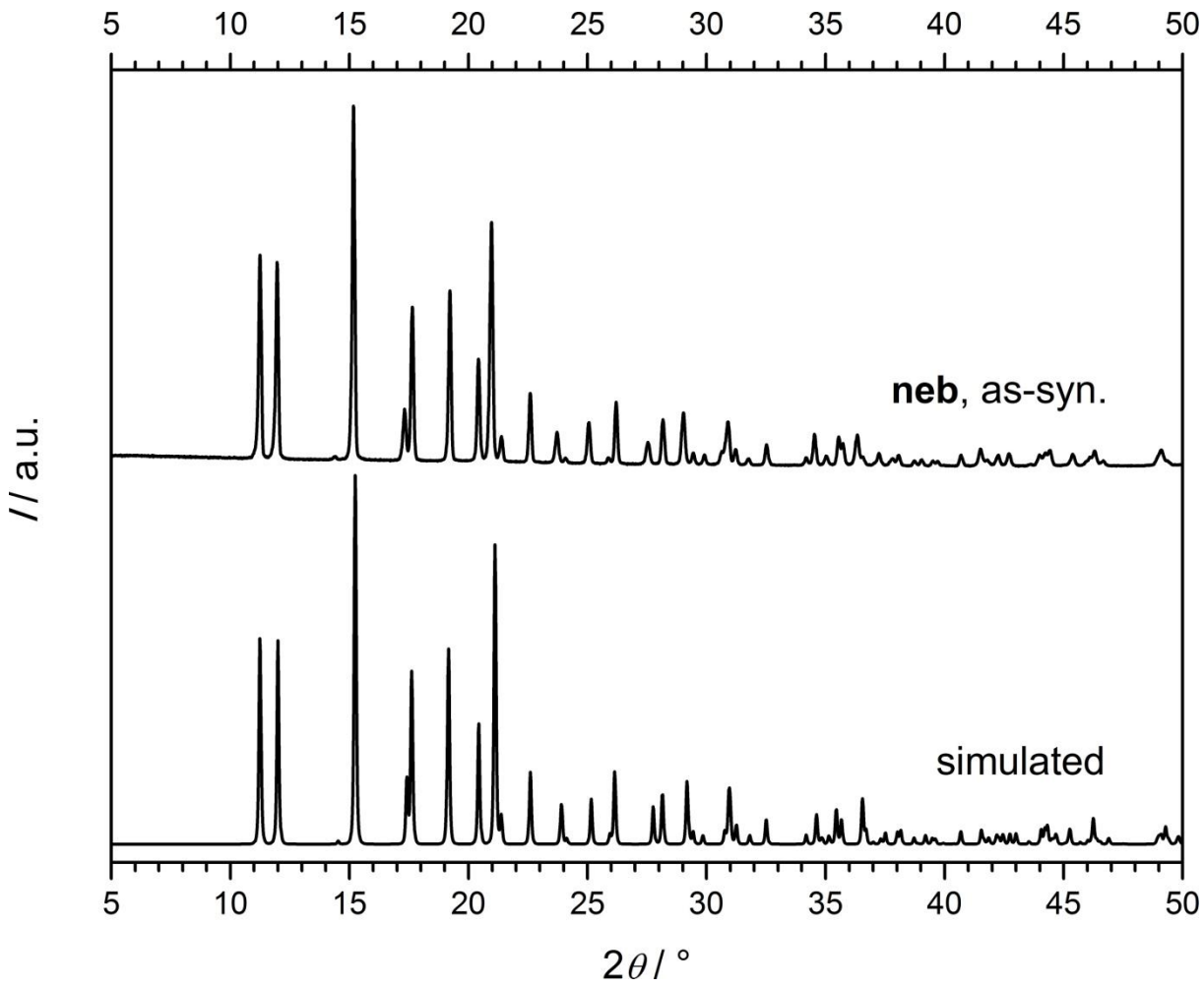

Fig. S6: Powder XRD pattern of [Zn(im)$_2$·0.5py]**-neb** recorded at room temperature. For comparison anXRD pattern simulated from structure data (see below) is also shown proving that pure-phase **neb** was obtained.

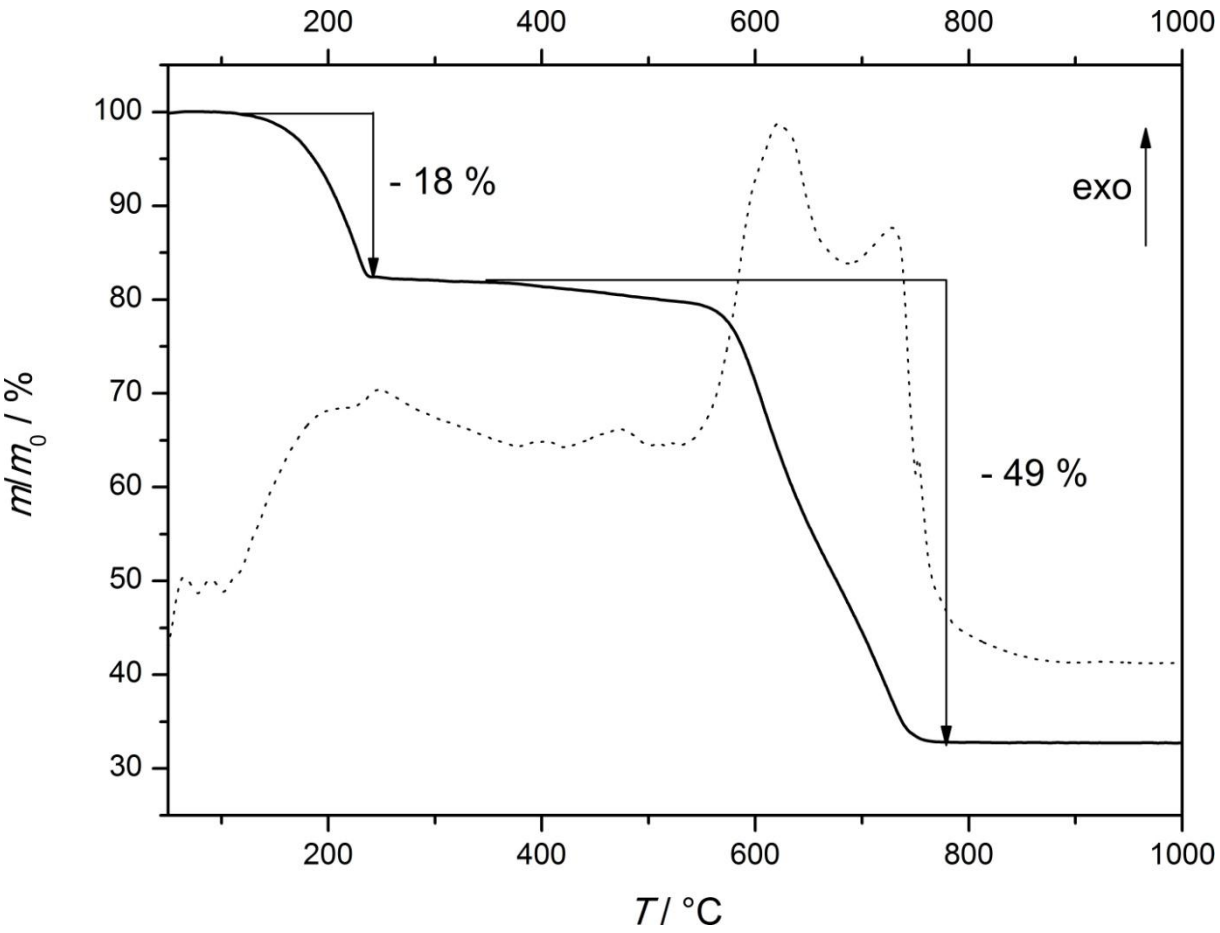

Fig. S7: TGA (solid line) and DTA (dotted line) curves measured from a $[Zn(im)_2 \cdot 0.5py]$**-neb** sample. The first mass loss (18 %) observed between approximately 120 and 250 °C can be assigned to pyridine molecules released from the structure and is in good a agreement with the calculated value (17 %) assuming a composition of $[Zn(im)_2 \cdot 0.5py]$. The second mass loss (49 %) beginning at approximately 400 °C can be assigned to the decomposition of the imidazolate ligands into volatile species and is also in good agreement with the calculated value (49 %). The inorganic residue is hexagonal ZnO as verified by XRD.

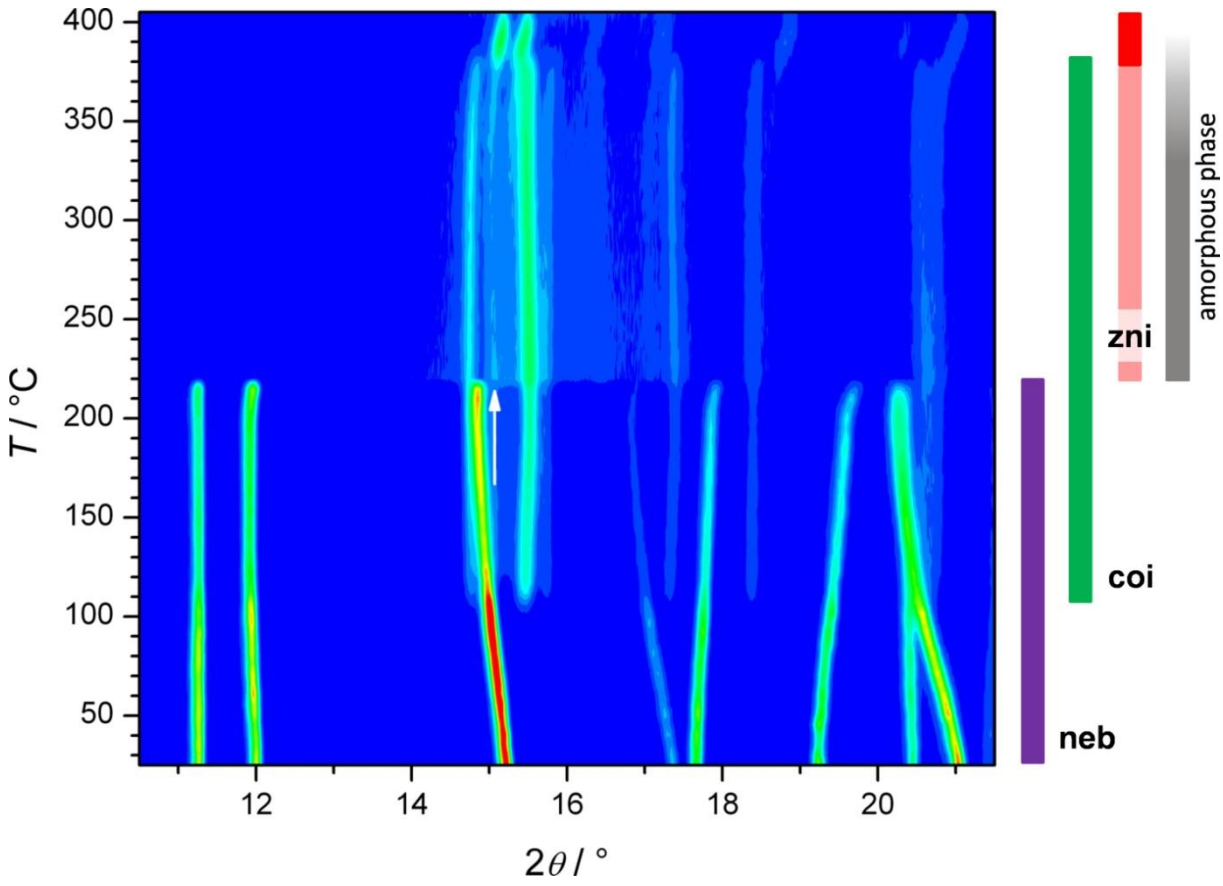

Fig. S8: XRD patterns of a [Zn(im)$_2$·0.5py]**-neb** sample recorded at variable temperatures. Starting at room temperature strong shifts of some reflections indicate that significant structural changes occur. At approximately 120 °C, the temperature at which the first loss of pyridine is observed on the TGA curve (Figure S8), the intensities of the **neb** reflections suddenly decrease and reflections of [Zn(im)$_2$]**-coi** appear. At approximately 220 °C, the temperature at which pyridine has escaped according to TGA, the **neb** reflections completely disappear while in addition to the **coi** reflections diffuse intensities (mainly between 15 and 16° 2θ) appear, indicating the generation of an amorphous phase. In addition a weak reflection (see arrow) of the [Zn(im)$_2$]**-zni** phase is seen. The amorphous phase and the **coi** phase transform into **zni** at approximately 360 °C. The XRD measurements prove that the **neb** phase collapses upon release of pyridine, *i.e.* the **neb** phase cannot be transformed into a permanently microporous material.

7. Single-Crystal Structure Analysis of [Zn(im)$_2$·0.5py]-neb

A suitable single crystal was mounted on a four-cycle Kappa ApexII CCD diffractometer (Bruker AXS) operated with graphite-monochomatised CuK$_\alpha$ radiation. The crystal was cooled to 173 K using an Oxford Cryostreams device. A numerical absorption correction based on indexing of the crystal faces was performed with the SADABS program (Bruker AXS). The structure was solved by direct methods and refined using all unique F_0^2 data with the programs SHELXS-97 and SHELXL-97,[7] respectively. All non-hydrogen atoms were refined with anisotropic displacement parameters. Hydrogen atoms were allowed to ride on the respective carbon atoms. Crystal data and some details of structure refinement are reported in Table S1. Full crystallographic data, atomic parameters, and interatomic distances are presented in a separate CIF file. CCDC reference number 889150.

Table S1. Crystal data and some details of structure refinement

formula	$C_{17}H_{17}N_9Zn_2$
formula mass	478.18
crystal system	orthorhombic
space group	*Fdd*2
Z	8
a / Å	18.5049(1)
b / Å	23.8735(1)
c / Å	9.3156(1)
V / Å^3	4115.42(6)
T / K	173
ρ / g·cm^3	1.543
μ(CuK$_\alpha$) / mm^{-1}	3.047
Flack parameter	0.08(4)
unique reflections	1710
R_{int}	0.0566
parameters refined	128
R1 [$\sigma(F_0^2) > 4\cdot F_0^2$]	0.0283
wR2 [all data]	0.0732
S	1.031
final $\Delta\rho_e$ [electron/Å^3]	+0.37 / –0.23

The crystal structure is based on the 3-dimesional 4-conneted **neb** net,[8] a 6^6 net that is closely related to the **dia** (diamond) and **lon** (lonsdaleite) structures as described previously for the Co analogue [$Co(im)_2 \cdot 0.5py$] by Tian *et al.*[6] The Zn cations sit on the nodes of the (distorted) **neb** net and are bridged by the imidazolate ligands. One kind of cage (tile) occurs which is bounded by 6 six-rings and occupied by a pyridine molecule the nitrogen atom of which is close to the centre of the cage (Figure S9). Via the six-rings the tetrahedral framework structure generates a 3-dimensional system of channels which run along the [001], [110], and [–110] directions (Figures S10 and S11). The ordered pyridine molecule is tightly fixed within the distorted cage (Figure S12). The small sizes of the six-ring windows in conjunction with the comparatively strong guest-framework interactions likely explain the fact that the framework does not withstand intact the escape of all pyridine molecules as evidences by TGA and powder XRD.

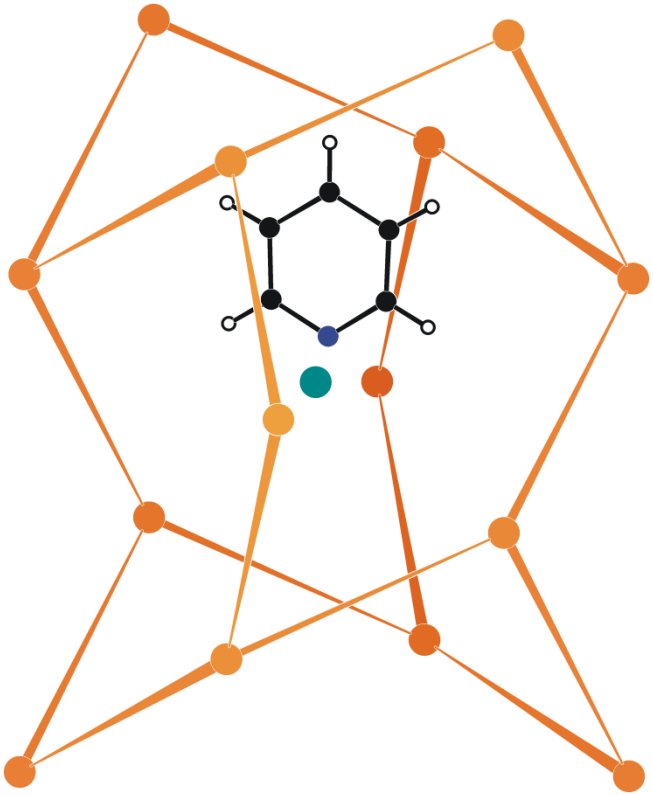

Fig. S9. Topological presentation of a distorted [6^6] cage with a pyridine molecule. Only the Zn atoms of the framework are shown. The crystallographic [001] direction runs vertically. Orange balls: Zn; green ball: centre of the cage; blue ball: Nitrogen; black balls: Carbon; open balls: Hydrogen.

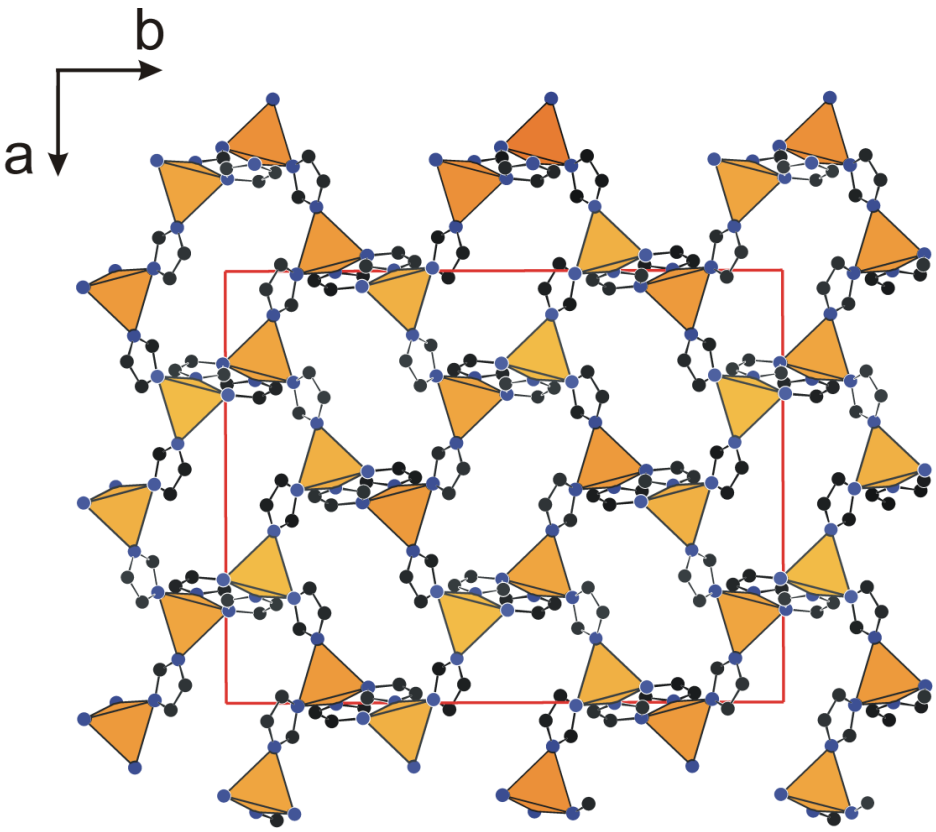

Fig. S10. Framework structure viewed parallel to [001], i.e. along one kind of channel. Orange tetrahedra: Zn-centred tetrahedra; blue balls: Nitrogen; black balls: Carbon. Hydrogen atoms and pyridine molecules are omitted.

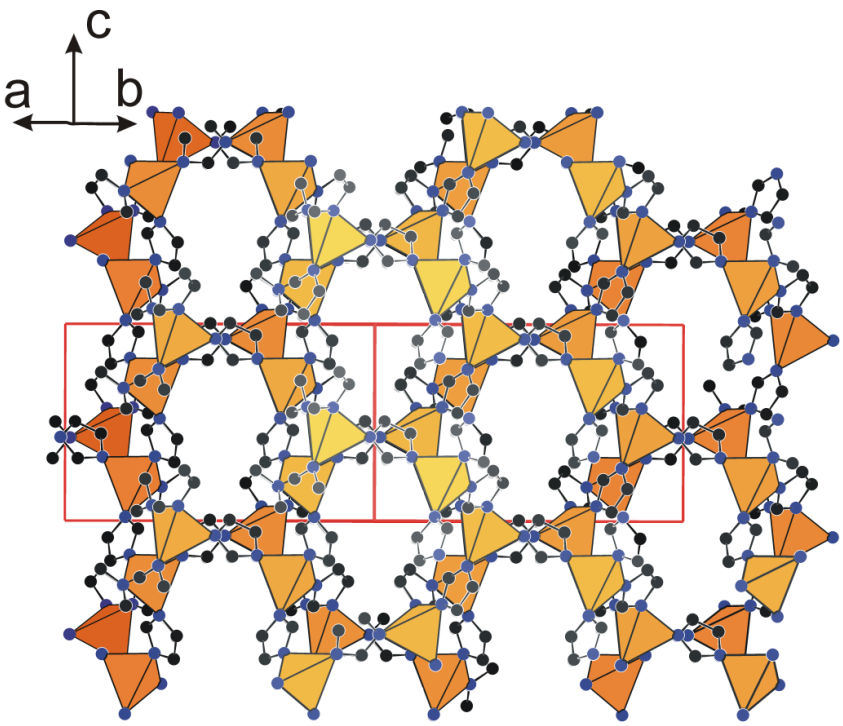

Fig. S11. Framework structure viewed parallel to [110], i.e. along one kind of channel. Orange tetrahedra: Zn-centred tetrahedra; blue balls: Nitrogen; black balls: Carbon. Hydrogen atoms and pyridine molecules are omitted.

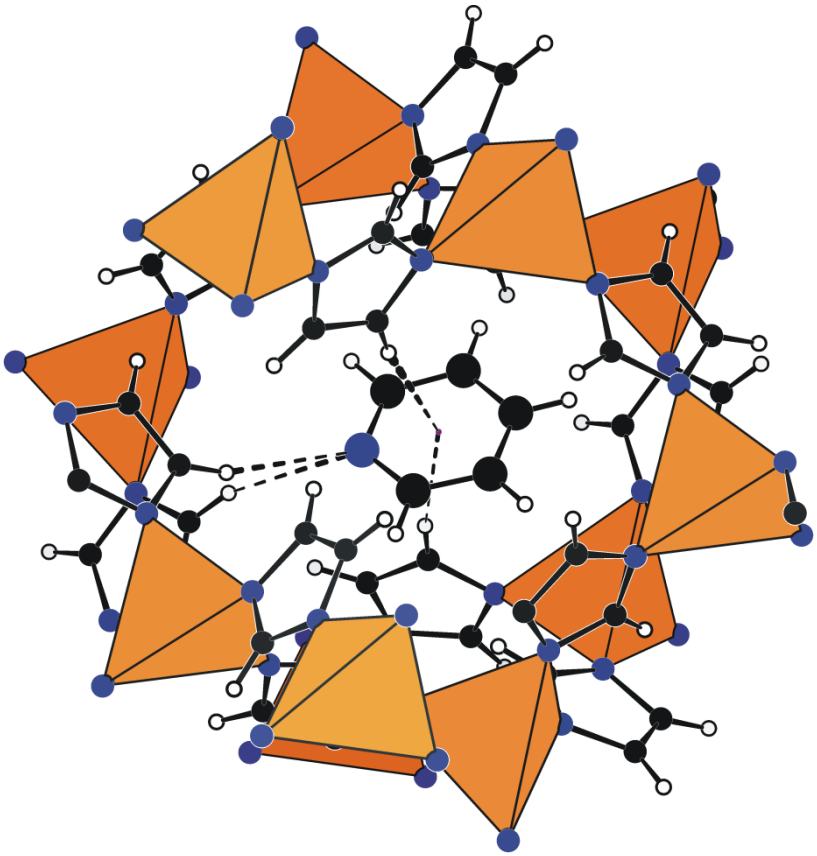

Fig. S12. Pyridine molecule with its framework environment. Orange tetrahedra: Zn-centred tetrahedra; blue balls: Nitrogen; black balls: Carbon; open balls: Hydrogen. The dashed lines indicate weak C–H···N(py) [*d*(C···N) = 3.655 Å, <(C–H···N) = 163°] and C–H···π(py) interactions [*d*(C···centroid) = 3.889 Å, <(C–H···centroid) = 171°].

8. Nuclear Magnetic Resonance (NMR) Spectroscopy of [Zn(im)$_2$·0.5py]-neb

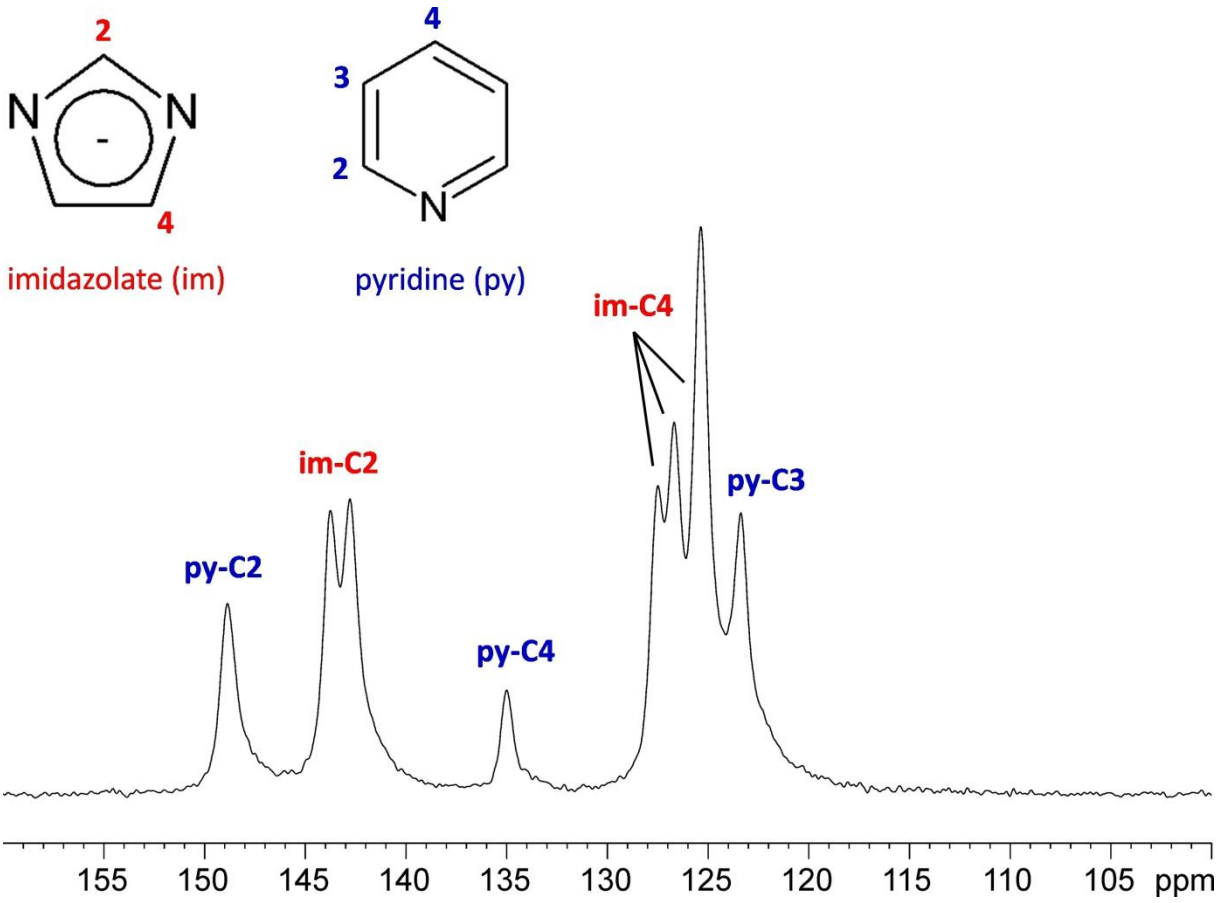

Fig. S13: CPMAS ^{13}C NMR spectrum with signal assignment. The multiplet structures of the imidazolate (im) carbon signals is in line with the two unique imidazolate ligands in the crystallographic asymmetric unit and their different structural environments. δ values: 148.91 (py-C2); 143.81 / 142.82 (im-C2); 135.05 (py-C4); 127.54 / 126.73 / 125.40 (im-C4); 123.51 (py-C3).[9,10]

9. References

(1) (a)J. M. Soler,E. Artacho, J. D. Gale, A. García, J. Junquera,P. Ordejón , D. J.Sánchez-Portal, *J. Phys.: Condens. Matter*,2002, **14**,2745; (b) P. Giannozzi, et al., J. Phys.: Condens. Matter, 2009, **21**, 395502.

(2) (a) J. P. Perdew, K. Burke, M. Ernzerhof, *Phys. Rev. Lett.*, 1996, **77**, 3865; (b) O. A. Vydrov and T. Van Voorhis, *J. Chem. Phys*., 2010, **133**, 244103; (c) R. Sabatini, E. Küçükbenli, B. Kolb, T. Thonhauser, S. de Gironcoli, *J. Phys.: Condens. Matter*, 2012, **24** 424209.

(3) N. Troullier , J. L. Martins, *Phys. Rev. B,* 1991, **43**, 1993.

(4) I. A. Baburin, S. Leoni, G. Seifert, *J. Phys. Chem. B,* 2008, **112**, 9537.

(5) E. C. Spencer, R. J. Angel, N. L. Ross, B. E. Hanson, J. A. K. Howard, *J. Am. Chem. Soc.*, 2009, **131**, 4022.

(6) Y.-Q. Tian, C.-X. Cai, X.-M. Ren, C.-Y. Duan, Y. Xu, S. Gao, X.-Z. You, *Chem. Eur. J.*, 2003, **9**, 5673.

(7) G. M. Sheldrick, *Acta Crystallogr. A*, 2008, **64**, 112.

(8) M. O'Keeffe, M. A. Peskov, S. J. Ramsden, O. M. Yaghi, *Acc. Chem. Res.*, 2008, **41**, 1782.

(9) A. A. Al-Badr, *Spectrosc. Lett.*, 1983, **16**, 613.

(10) M. Hansen, H. J. Jakobsen, *J Magn. Res.*, 1973, **10**, 74.